76th International Astronautical Congress, Sydney, Australia, 29 September-3 October 2025.

IAC–25–C1,IPB,8,x102383

Design of elliptic orbit constellations for solar reflectors for terrestrial solar energy enhancement

Onur Çelik
Faculty of Aerospace Engineering, Delft University of Technology, Delft 2629 HS, The Netherlands

Orbiting solar reflectors (OSR) are large, thin, flat and ultralightweight structures proposed to extend the operational hours of solar power farms (SPF) beyond the daylight hours by locally illuminating them at night from orbit. They operate with the principle of intercepting incoming sunlight and reflecting an image of the solar disk onto a ground target by tracking. It has been previously shown that a constellation of modest number of OSR in circular, Sun-synchronous low-Earth orbits can increase the efficiency of terrestrial SPF considerably [1]. The design of such constellations typically relies on circular orbits due to the reduced complexity of orbit selection and optimising the constellations for a given objective, where analytical expressions are available for simple constellation patterns. Introducing nonzero eccentricity to orbit shape immediately multiplies the complexity of the optimisation problem as the number of available orbits are in principle infinite, but their employment in the design would enhance the flexibility in mission design and may offer an improved performance. This paper therefore investigates the design of optimal OSR constellations with elliptic Sun-synchronous orbits with an objective to maximise the daily quantity of energy delivered. An analytical approach is used to simplify the design process by placing reflectors in different orbit planes that allow reflectors to follow the same pass geometry over a given target, reducing the constellation optimisation to effectively a single groundtrack optimisation, carried out by a genetic algorithm for full orbital element space except semi-major axis. The results demonstrate that introducing eccentricity at three different semi-major axis values increase the daily quantity of energy delivered by up to 20%, offering flexibility in constellation design with reduced complexity that can be applied applications beyond terrestrial space-based solar power.

1. Introduction

Orbiting solar reflectors are proposed to enhance the terrestrial solar power farm output by locally illuminating them in the hours of sunlight unavailability [2]. This large, ultra-lightweight and flat structures are closely related to solar sailing and other planar technologies termed as space sailing [3, 4] and initially proposed by Hermann Oberth [5]. Together with other wireless power beaming options [6], the concept of orbiting solar reflector has been explored by NASA and other researchers for terrestrial solar energy, street illumination and the enhancement of agriculture among the other applications [7, 8, 9]. In parallel with the developments in the solar sailing technology and the other large gossamer structure such as deployable antennas, the orbiting solar reflector concept has also been tested in space by a 20-m diameter disk reflector by the Russian space agency as part of Znamya-2 experiment in 1993 [10]. A comprehensive review on orbiting solar reflectors can be found in Çelik et al. (2022) [2].

The demand for global clean energy, reducing launch costs and the other advancements in space technology such as in-orbit manufacturing and assembly allowed the concept of orbiting solar reflector to be re-explored [2]. Fraas et al published a number of studies on the orbiting reflector concept, proposing it as a low-cost solar energy option [11]. Bonetti & McInnes (2019) proposed a two reflector constellation to illuminate solar power farms in three locations globally to enhance solar power farm output [12]. The reference architecture by Viale et al. (2022) proposes a five-reflector in train to illuminate twelve existing solar power farms on the Earth and offers a comprehensive study on attitude control, reflector structure and the economics of space-based solar power with orbiting reflectors [13]. Viale et al. (2022) also presented in a technology roadmap for the commercial deployment of orbiting solar reflectors, offering a step-by-step approach from balloon experiments to small-scale technology demonstrator with CubeSats around the Earth and the Moon [14]. To that end alternative applications of orbiting reflectors also exist to survive the lunar night [15, 16] and climate services as sunshades around the Earth, integrated with space-based solar energy [17]. Beyond the academia, European Space Agency's SOLARIS programme ex-

plored the concept under the name *Direct Sun Reflection* and demonstrated its viability for terrestrial clean energy applications.* The US-based start-up ReflectOrbital now plans to launch a constellation of small reflectors to deliver sunlight terrestrial targets for various illumination applications.†

Indeed, a constellation of orbiting reflectors can significantly enhance terrestrial solar power generation. Çelik & McInnes (2024) demonstrated that a constellation of ten 1-km diameter reflectors at at 1000-km circular orbits can provide solar energy equivalent to a terrestrial solar power farm, but distributed globally [1]. The authors have used a Walker constellation pattern [18] and modified it such that it is synchronised with Earth's rotation and the precession by the Earth's oblateness effect, such that each reflector's pass over a target is the same, offering a scalable, continuous, controllable and predictable solar energy delivery. The application of circular orbits simplifies the problem; however, it also limits the available solution space for orbiting reflector constellations. This is because the reflected solar energy delivery is dependent on its distance to the ground [19, 20], i.e., the size of the solar image, therefore solar power density, is dependent on this distance. Lower altitudes enable higher solar power density but shorter pass durations, and vice versa. The trade-off for the altitude of solar reflector constellations is also more complicated when one considers the atmospheric drag effects and space debris consideration [21]. Therefore, elliptical orbits appear as an alternative, which would allow partial time in lower altitudes for solar power density, but also in higher altitudes that is less affected by the atmospheric drag and away from densely populated orbits. Despite a number of proposal for the benefits of elliptical orbit constellations [22, 23, 24, 25], they have not been employed widely due to the immediately expanded solution space with infinite possible orbits in principle. Bonetti & McInnes (2019) considered a highly constrained design space with solar radiation pressure assisted Sun-synchronous anti-heliotropic orbits and Flower constellations [26] while they have also simplified the problem by placing three equally spaced ground targets [12]. Even if constraints such as sun-synchronicity is considered to constrain the search space, the dependency of orbit inclination to the eccentricity makes the optimisation of a constellation for a given objective non-trivial, particularly in the case of non-equally spaced ground targets.

This paper investigates the design of orbiting solar reflector constellations with the inclusion of elliptical orbits and assesses their effectiveness for terrestrial solar energy enhancement. Building upon the author's previous work [1], a framework for constellation design is introduced, which includes full Keplerian orbital element space except the semi-major axis as optimisation parameters. A single satellite per orbit is considered and the remaining satellites are distributed in the successive orbit planes based on a phase angle that ensures the same pass geometry for all satellites. This means that only the first reflector's orbit needs to be optimised. This was carried out by employing a genetic algorithm with an objective to maximise the total quantity of solar energy delivery per day, by including a realistic model for reflected solar energy delivery [20] and existing solar power farms are included in the optimisation. Initial exploration of elliptic orbit space is performed with polar orbits to remove eccentricity-inclination coupling for comparisons with circular orbits, which is extended to Sun-synchronous orbits. Three different semi-major axis values are considered and the results are compared against respective circular orbits. Finally, the results are discussed in the context of space mission design and terrestrial solar energy enhancement.

This paper is structured as follows: A model of reflected solar energy delivery will be presented next and followed by a model constellation design in Sec 3. The optimisation procedures will be discussed in Sec 4 and the results of the optimisation will be presented in Sec 5. A discussion will be offered in Sec. 6 and finally the conclusions will be presented in Sec. 7.

2. Reflected solar energy delivery from space

$$P_{SPF} = \chi(t) I_0 \frac{A_M}{A_{im}(t)} A_{SPF} \cos\frac{\psi(t)}{2} \qquad (1)$$

where I_0 is the solar constant which is assumed to follow an inverse-square law with the distance from the Sun and equal to 1.37 GWkm^{-2} at the mean distance between the Earth and the Sun, i.e. 1 Astronomical Unit (AU). A_M, A_{SPF}, A_{im} are the areas of the reflector, solar power farm and the projected image of the Sun (i.e., illuminated region) on the ground. A_M and A_{SPF} have fixed areas, but A_{im} is an elliptical area whose size is a time-dependent function that can

*SOLARIS website: `https://www.esa.int/Enabling_Support/Space_Engineering_Technology/SOLARIS/SOLARIS2`, Accessed September 12, 2025

†ReflectOrbital website: `https://www.reflectorbital.com/`, Accessed September 12, 2025.

be written as [20]:

$$A_{im}(t) = \pi a(t)b(t) = \pi \frac{[d(t)\tan(\alpha/2)]^2}{\sin\epsilon(t)} \quad (2)$$

where d denotes the magnitude of the slant range vector measured from the topocentric-horizon reference frame (THF) of the ground target such as a solar power farm and α denotes the angle subtended by the Sun, approximately 0.0093 rad at 1 AU. ϵ denotes the elevation angle measured from the local horizontal, defined again in the topocentric frame of the ground target and is given by [20]:

$$\epsilon(t) = \arcsin\frac{z_{THF}(t)}{d(t)} \quad (3)$$

where z_{THF} is the z-axis component of the slant range vector and given in [20]. The details of the derivation of Eqs. 2 and 3 will not be provided in this paper for conciseness, but in a recent paper Çelik & McInnes presented detailed analytical derivations as a function of orbital elements for both as a three-dimensional vector model by including the Earth's rotation and the Earth's oblateness perturbation for applications to Sun-synchronous orbits [20]. A simplified scalar model is also presented for polar orbits in Çelik & McInnes [19].

The time-dependent atmospheric transmission efficiency, $\chi(t)$, Eq. 1 is provided with the following empirical relationship [27]:

$$\chi(t) = 0.1283 + 0.7559e^{-0.3878\sec(\pi/2-\epsilon(t))} \quad (4)$$

Finally, $\psi(t)$ denotes the time-dependent the angle of incidence, and defined as the angle between the incoming and outgoing sunlight.

The quantity of the energy delivered, E to the surface can then be calculated by integrating Eq. 1, such that:

$$E = \int_0^t P_{SPF}\mathrm{d}\tau \quad (5)$$

where t is time. t may be the pass duration over a solar power farm, T_{pass}. The quantity of energy delivered will be used as the objective for the optimal constellations, which are presented next.

3. Constellation design

Satellite constellations are typically designed in the inertial reference frame, with prime example being Walker constellations. However it may be preferrable to place satellites in a constellation in rotating reference frame, first, as it represents a more realistic case and second, as a mission requires subsequent satellites in a constellation to be repeating the same groundtrack. Such a problem is presented in Çelik & McInnes (2024) for orbiting solar reflector applications and will be summarised here with extensions to elliptical orbits. To analyse the details of this problem, first Walker constellations will be considered [18]. Walker constellations are one of the most common orbit constellations [18], widely used for applications such as navigation [28]. The satellites in Walker constellations would possess the same orbit radius, eccentricity and inclination, and would be distributed in the right ascension of the ascending node (RAAN) and mean anomaly space equally for a given number of orbits and satellites and a phasing parameter [18]. The state-space form of this distribution can be expressed as follows [18]:

$$\begin{bmatrix} N_o & 0 \\ N_p & N_{so} \end{bmatrix} \begin{bmatrix} \Omega_{mn} - \Omega_{11} \\ M_{mn} - M_{11} \end{bmatrix} = 2\pi \begin{bmatrix} m-1 \\ n-1 \end{bmatrix} \quad (6)$$

where N_o denotes the number of orbits, N_so denotes the number of satellites per orbit, N_p denotes a phasing parameter that takes integer values in the range $N_p \in [0\ N_o\text{-}1]$. Ω and M are RAAN and mean anomaly, respectively, and m and n are the indices of orbits and satellites, respectively. Ω and M can also be rewritten as [18]:

$$\Omega_{mn} = \Omega_{11} + \frac{2\pi}{N_o}(m-1) \quad (7a)$$

$$M_{mn} = M_{11} + \frac{2\pi}{N_{so}}(n-1) - \frac{N_p}{N_{so}}\Delta\Omega \quad (7b)$$

where $\Delta\Omega = \Omega_{mn} - \Omega_{11}$. The general form of the Walker constellation given in Eq. 7 distributes the orbit planes equally across the Earth by $2\pi/N_o$ term. This is not necessarily useful for orbiting solar reflector type applications, as the primary aim is to deliver solar energy at dawn/dusk around the terminator region. It is also not clear what other angle can replace 2π in Eq. 7a. As the aim of the reflector constellations is to ensure the same geometry across all reflectors, the separation between the orbit planes needs to be set accordingly and the reflector's placement in the constellation orbits should allow synchronisation with the Earth's rotation, such that:

$$\Delta\Omega = \omega_E t_{n+1} = \frac{\omega_E}{\omega_o}\phi \quad (8)$$

where ω_E is the Earth's rotation rate, $\omega_E = 7.272 \times 10^{-5}$ rad/sec. However, if the Earth's oblateness is taken into account, the orbit plane of all reflectors will also shift due to this perturbation. In this paper,

the Earth's oblateness up to the second order (i.e., $J_2 = 1082.63 \times 10^{-3}$) is considered, whose impact on RAAN can be expressed as the rate of change [29]:

$$\dot{\Omega}_{J_2} = -\frac{3}{2} J_2 \left[\frac{\sqrt{\mu} R_E^2}{(1-e^2)^2 a^{7/2}} \right] \cos i \tag{9}$$

where e and i denote the orbit eccentricity and inclination, respectively. Therefore, the shift in the orbit plane of the subsequent spacecraft by considering the J_2 effect can be expressed as:

$$\Delta\Omega_{J_2} = -\dot{\Omega}_{J_2} t_{n+1} = -\dot{\Omega}_{J_2} \frac{\phi}{\omega_o} \tag{10}$$

It is worth noting that the orbit angular rate will also be altered as a result of the Earth's oblateness, due to the change in the orbit period, which can be expressed as:

$$T_{J_2} = T \left[1 - \frac{3}{2} J_2 \frac{R_E^2}{p^2} - \frac{3}{4} J_2 \frac{\left(4 - 5\sin^2 i\right) R_E^2}{p^2} \right] \tag{11}$$

where p is semi-latus rectum, i.e. $p = a(1-e^2)$. Finally, combining Eqs. 8 and 10 would yield the angular separation between orbit planes, such that:

$$\Delta\Omega = (\omega_E - \dot{\Omega}_{J_2}) \frac{\phi}{\omega_{o,J_2}} \tag{12}$$

where ω_{o,J_2} is the J_2 altered orbit angular rate and is equal to $\omega_{o,J_2} = 2\pi / T_{J_2}$. Then, if the 2π term at the right-hand side of Eq. 7a is redefined as some angle η_Ω, it can be found as:

$$\eta_\Omega = (\omega_E - \dot{\Omega}_{J_2}) \frac{\phi}{\omega_{o,J_2}} N_o \tag{13}$$

If, then, a circular orbit constellation is considered with six orbit planes at 1000-km altitude and $\phi = 15\,\text{deg}$ separation between them, η_Ω would become $6.58\,\text{deg}$. Hence, the orbit planes would be equally distributed in this range. In a case, where the orbit is unperturbed, an initial shift in mean anomaly by ϕ would ensure that subsequent reflectors would follow the same pass geometry. However, the Earth's oblateness also rotates the orbit itself (or shifts the start/end point of the orbit), such that [29]:

$$\dot{\omega}_{J_2} = -\frac{3}{2} J_2 \left[\frac{\sqrt{\mu} R_E^2}{(1-e^2)^2 a^{7/2}} \right] \left(\frac{5}{2} \sin^2 i - 2 \right) \tag{14}$$

where ω denotes the argument of pericentre. Then the shift in ω can be described as:

$$\Delta\omega = -\dot{\omega}_{J_2} t_{n+1} = -\frac{\dot{\omega}_{J_2}}{\omega_{o,J_2}} \phi \tag{15}$$

$\Delta\omega$ can now be combined with the unperturbed mean anomaly shift $M - \phi$ and orbit plane separation $\Delta\Omega$ in Eq. 12 to describe the distribution of reflectors in a constellation of m orbit planes with a *single* reflector in each orbit:

$$\Omega_m = \Omega_{11} + \left(\frac{\omega_E - \dot{\Omega}_{J_2}}{\omega_{o,J_2}} \right) \phi(m-1) \tag{16a}$$

$$M_m = M_{11} - \left(1 + \frac{\dot{\omega}_{J_2}}{\omega_{o,J_2}} \right) \phi(m-1) \tag{16b}$$

Again, the parameter n is not in the set of equations as there is one reflector per orbit, which is due to the second term in the right-hand side of Eq. 7b becoming zero for a single reflector per orbit.

Equation 16b can be expanded to include more satellites per orbit by including the same term in Eq. 7b by replacing 2π term by some angle η_M for further customisation of the constellation:

$$\Omega_{mn} = \Omega_{11} + \left(\frac{\omega_E - \dot{\Omega}_{J_2}}{\omega_{o,J_2}} \right) \phi(m-1) \tag{17a}$$

$$M_{mn} = M_{11} + \frac{\eta_M}{N_{so}}(n-1) - \left(1 + \frac{\dot{\omega}_{J_2}}{\omega_{o,J_2}} \right) \phi(m-1) \tag{17b}$$

The description of the constellation orbits in Eqs. 16 and 17 ensures that the reflectors will exhibit the same pass geometry as they pass over a solar power farm. Even if there is more than one reflector per orbit, the second reflector in the subsequent orbit would also follow the same geometry as the second reflector in the previous orbit plane. The advantage of the same pass geometry is that, it would be no longer necessary to consider all reflector satellites in all orbit planes in the constellation optimisation, but the first reflector's orbit. The orbits and mean anomaly values of the rest of the reflector satellites can then distributed according to Eqs. 16 and 17 and the result can be generalised. But care must still be taken to set the optimisation problem to ensure the range of orbits is appropriately placed in the terminator region to avoid conditions such as eclipses, which is discussed next.

4. Groundtrack optimisation

The optimisation problem tackled in this paper incorporates the energy delivery process and the placement of the orbit plane in the orbital element space. For both polar and Sun-synchronous orbits, a single reflector initially at true anomaly $TA = 0\,\text{deg}$ is considered. Recall that the setting of the constellation

problem in Eqs. 16 and 17 ensure that reflectors in subsequent orbits would follow the same pass geometry over the solar power farms as the reflectors in the first orbit. Before the details of the optimisation process is presented, first the selection of the solar power farms will be summarised.

4.1 Solar power farms

Solar power farms (SPF) in this paper are selected from some of the largest operational and under-development projects with nameplate capacity greater than 550 MW as of 2020, first summarised in Viale et al. (2023) [13]. In addition, this paper also considers a number of hypothetical solar power farms. The potential benefits of additional solar power farms that are strategically placed near the groundtrack of a selected reflector orbit and high-insolation regions were previously discussed in Viale et al. (2023) in enhancing the terrestrial solar energy generation [13]. In this paper, this will be considered alongside existing solar power farm projects to assess that enhancement. The SPF considered in this paper are presented alongside a yearly mean insolation map (covering 1990-2004) in Fig. 1.

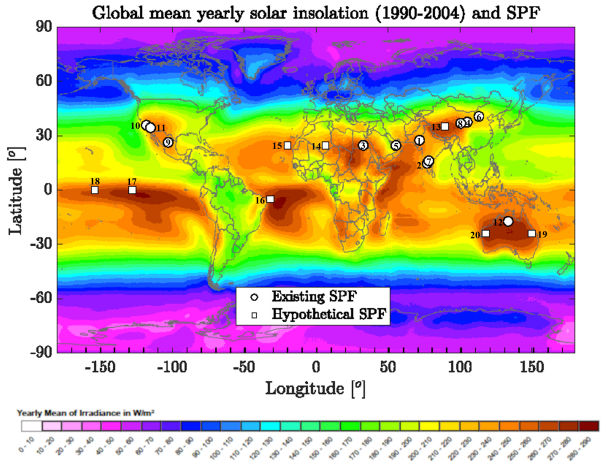

Fig. 1: Solar power farms considered in this work (from [1]). Hypothetical SPF is provided for reference but not used in the analysis.

Figure 1 shows how the existing SPF projects are placed in favourably insolated geographical locations. For hypothetical farms, a similar approach is taken, but longitudes of hypothetical SPF are also chosen by considering the longitudinal shift of the ground track on the surface of the Earth after each orbit. This is done so by considering 1000-km circular orbit presented in Çelik & McInnes (2024) not changed for comparison purposes. In elliptical orbits, the longitudinal shift would be variable for each orbit as the shift due to the Earth's oblateness effect is dependent on both eccentricity and inclination, except the perfectly polar orbits.

Considering eastward Earth rotation at a rate of ω_E and westward rotation due to the J_2 effect, $\dot{\Omega}_{J_2}$, the orbit ground track would shift approximately $(\omega_E - \dot{\Omega}_{J_2})T_{J_2}$. For the 1000-km orbit altitude, this will mean that the westward groundtrack shift for a Sun-synchronous orbit and polar orbit at this altitude would be 26.7 deg and 26.3 deg, respectively. Therefore, the longitudinal separation between two consecutive hypothetical SPF is considered to be 26.7 deg as SSOs are more relevant for orbiting solar reflector applications and the difference between SSO and polar orbits is small in terms of ground track shift. Latitudinal placement is more related to nearby existing SPF, insolation properties, proximity to land and generally attempting to avoid an orbit groundtrack passing over multiple farms at the same time or in quick succession to ensure distinctive passes. The locations of the SPF are listed in Table 1.

Table 1: Selected solar power farms in this paper (from [1]).

#	Solar power farm (SPF)	Capacity [MWh]	Land size [km^2]	Coord. (lat., lon) [deg, deg]
	Existing solar power farm projects			
1	Bhadla	2700	160	27.5, 71.9
2	Pavagada	2050	53	14.7, 77.2
3	Benban	1650	37	24.7, 32.8
4	Tengger	1547	43	37.6, 105.04
5	Noor Abu Dhabi	1177	8	24.6, 55.4
6	Datong	1070	N/A	40.7, 113.1
7	Kurnool	1000	24	16.15, 78.4
8	Longyangxia	850	14	36.9, 100.5
9	Villanueva	828	24	26.3, -102.9
10	Solar Star I&II	747	13	35.8, -118.15
11	Topaz	550	19	34.4, -115.2
12	Sun Cable	17000	105	-17.29, 133.5

4.2 Optimisation process

The optimisation process is as follows: First, for given orbit parameters, the orbit pass geometry is calculated for 24h in terms of its elevation angle for each of the solar power farms presented in Table 1. After an initial numerical propagation of the orbit, the elevation history is generated for each target solar power farm in their local topocentric horizon reference frame. If the maximum elevation angle reached over a ground target is greater than 60 deg, these

instances are recorded and the solar power farm is considered serviceable. Such a pass would typically occur twice a day for low-Earth orbit satellites. Solar power farms are not serviced if the maximum elevation reached is below this given threshold and skipped. this threshold is distinguished for each pass, i.e., as SPF can be serviced in one pass and not serviced in the other, instead of discarding the target entirely. For the passes that satisfy the 60 deg requirement, the quantity of energy delivered is calculated. This follows the procedures discussed in Çelik & McInnes (2022, 2023) [19, 20] with the equations presented in Sec. 2 and includes Earth rotation and oblateness, geometric and atmospheric losses in the energy delivery process [19, 20].

This procedure is performed for all reflectors (if there is more than one) and for all solar power farms. Finally, the quantity of total energy delivered per day is calculated. A limitation of this approach is the closely located solar power farms, which can be seen in Fig. 1. In this situation, it was observed that often the groundtrack passes over multiple closely located SPF satisfying the 60 deg requirement, which results in the over-calculated quantity of energy delivered within the optimisation function. While it is not necessarily a problem, one of those overlapping passes will need to be selected as servicing two SPF is not feasible due to attitude control requirements [13]. One of those will always provide the highest quantity of energy delivered, which is selected while the others are removed as infeasible in the post-processing.

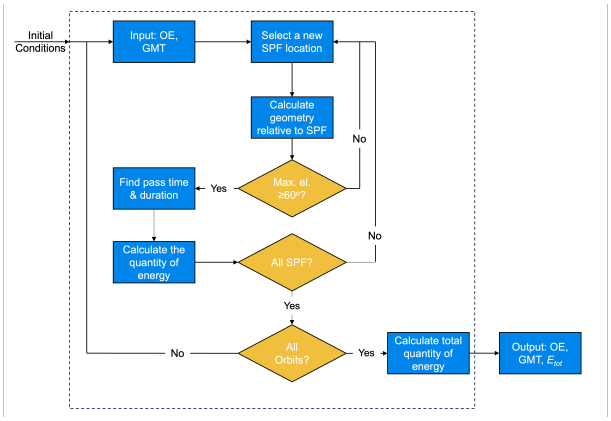

Fig. 2: Diagram of the optimisation process. OE and GMT denote orbital elements and Greenwich mean time respectively.

The objective of the optimisation is to maximise the total quantity of energy delivered per day. Due to elliptical orbits considered, there will be multiple optimisation parameter considered throughout the paper, with increasing complexity. Initially, semi-major axis, eccentricity, argument of periapsis values will be fixed and the two optimisation parameters will be the right ascension of the ascending node Ω and the initial Greenwich meridian, $\theta_{G,0}$. The latter parameter appears relatively arbitrary as it only determines when the orbit starts during a day but necessary to find the optimal solution. This initial exploration phase will allow for a comparison between circular orbit constellations explored in Çelik & McInnes (2024) [1]. The range of Ω is selected based on the eclipse considerations and a range extending by β on either side of the terminator line defined at $\pi/2$ from the x-axis in the ECI frame. As for $\theta_{G,0}$, the range is selected between -90 deg and 90 deg measured from the x-axis in the ECI frame or approximately 6:00 am-6:00 pm GMT.

The optimisation will increase in complexity for fixed semi-major axis values and by equating the argument of periapsis value to 0, and an eccentricity, right ascension of the ascending node and initial Greenwich meridian that maximises the daily total quantity of energy will be sought. Finally, the argument of periapsis value will be an optimisation parameter as well and for a given semi-major axis of the orbit, the orbit elements that maximises the daily total quantity of energy will be sought. For all cases, true anomaly will be equal to zero. The optimisation procedure will be carried out for both existing and hypothetical solar power farms. Table 2 summarises some of the parameters in the optimisation process.

Table 2: Parameters of the optimisation problem

Orbital parameters	
Semi-major axis [km]	7378.2, 7500, 8000
Inclination [deg]	90 (Polar), Various (SSO)
Reflector parameters	
Diameter [km]	1
Reflectivity [-]	1
Solar power farms	
Diameter [km]	10
Location	Table 1
Optimisation parameters	
Objective function	$-E_{\text{tot}}$
Variables	$e \in (0,\ e_{max}(r_{p,min})]$ $\omega \in [0,\ 360]$ deg $\Omega \in [90-\beta,\ 90+\beta-\eta_\Omega]$ deg $\theta_{G,0} \in [-90,\ 90]$ deg

The single-objective optimisation is performed using a genetic algorithm [30] and implemented in `MAT-`

LAB through its ga() function.[‡] A genetic algorithm is based on the principle of evolution to reach the best result (or global optimum) via stochastically generated populations via crossovers and mutations. Genetic algorithms are commonly used in constellation optimisation when the problem of minimising an objective function with the best distribution of satellites is not immediately apparent. For the problem at hand in this paper, the optimisation does not include many satellites, orbits or number of planes, but the pass geometry over the listed solar power farms and the associated quantity of energy deliverable to those cannot be found trivially, hence the genetic algorithm becomes a suitable choice. For the different settings available for ga() in MATLAB, initial parameter space is created based on a uniform distribution with scattered crossover and stochastic uniform selection of parents at each step. For the mutations, an adaptive feasible mutation option is selected, which generates random search directions and is adaptive to the success of each generation. The function and constraint tolerances are 10^{-6} and 10^{-3}, respectively. The maximum generations in an optimisation is set to 50 after an initial exploration of the problem. After presenting procedures and tools in the optimisation process, the results of the groundtrack optimisation can be presented in the next section.

5. Optimised orbits and their properties

5.1 Polar orbits

The orbit optimisation is performed for Sun-synchronous orbits as they are more relevant for orbiting reflector applications. However, due to the coupling between eccentricity and inclination in SSOs, the comparison is between circular and elliptical orbits is not straightforward. In order to assess the effectiveness of elliptical orbits in reflector constellations, the initial analysis is therefore performed with polar orbits to remove the effect of the Earth's oblateness. The results for 7378.2 km radius (i.e., 1000 km altitude) circular orbit are also available in Çelik & McInnes (2024) [1]. For comparison, semi-major axis length $a = 7378.2$ km is selected. The minimum periapsis length is limited to 600 km to avoid enhanced atmospheric effects, which results in a maximum eccentricity value of 0.0542. A grid search is then performed as part of the optimisation for eccentricity values e =[0.01, 0.025, 0.05] and AoP values ω = [0, 90, 180, 270] deg. In this first step, only RAAN and GMT values are sought that maximises the total daily quantity of energy delivered. The results on this analysis is provided in Table 3.

Table 3: Polar orbit results at three eccentricity (e) and four different argument of periapsis (ω) values. Semi-major axis length (a) is 7378.2 km

e [-]	ω [deg]	Ω [deg]	θ_{GMT} [deg]	E_{tot} [MWh]	$E_{tot,pp}$ [MWh]
0.01	0	89.05	14.65	461.9	338.0
0.025	0	87.47	-5.46	418.8	313.7
0.05	0	95.83	18.13	432.1	339.6
0.01	90	107.98	-44.87	442.7	331.2
0.025	90	85.03	-56.32	437.3	336.9
0.05	90	80.91	-5.31	431.4	333.6
0.01	180	102.32	-4.39	451.6	335.7
0.025	180	89.97	-10.36	462.9	362.8
0.05	180	101.35	-6.03	383.9	300.8
0.01	270	94.49	-5.53	445.7	335.6
0.025	270	72.31	-2.69	436.5	338.2
0.05	270	83.05	-10.75	435.5	343.3

The total daily delivered energy (E_{tot}) is found between 452.9-454.3 MWh in Çelik & McInnes (2024) [1]. Another result is defined in the last column, $E_{tot,pp}$, which refers to the post-processed results after removing overlapping passes as explained in the previous section. The range of $E_{tot,pp}$ in Ref. [1] was 333.3-334.7 MWh. The results show that for elliptical orbits E_{tot} range is larger, between 383.9 MWh and 462.9 MWh and $E_{tot,pp}$ ranges between 300.8 MWh and 343.3 MWh. From an optimisation perspective, this results show that a comparable performance to circular orbits can be obtained in E_{tot} by elliptical orbits with moderate eccentricities. For post-processed results ($E_{tot,pp}$), the interpretation is the similar on average, but better performance can be obtained in majority of the cases of varying degrees. An overhead pass equivalent energy can be defined from 1000-km altitude circular orbit over 10-km diameter solar power farm as 35.2 km [19]. Then, at least 10% of one-pass equivalent improvement is possible by elliptical orbits, demonstrating the benefit of elliptical orbits for flexibility in mission design and improved performance.

The results in Table 3 are only investigated for four AoP values. If the AoP is also added as one of the optimisation parameters, the results can be improved as presented in Table 4.

Table 4: Optimisation results for polar orbits at three different eccentricity values. a = 7378.2 km

e [-]	ω [deg]	Ω [deg]	θ_{GMT} [deg]	E_{tot} [MWh]	$E_{tot,pp}$ [MWh]
0.01	178.21	78.22	-16.50	455.5	374.4
0.025	171.67	94.08	-8.59	462.2	356.2
0.05	249.96	93.43	-6.46	457.4	354.7

[‡]Available at https://uk.mathworks.com/help/gads/ga.html, Accessed August 29, 2025

The final ω values in Table 4 are in agreement with the results on Table 3, i.e., e=0.1 and e=0.025 results are close ω = 180 deg and e=0.05 result is close to ω =270 deg. All E_{tot} results are higher than circular orbit results [1]. The post-processed results are approximately more than 60% higher for all eccentricity values, which means nearly another pass equivalent energy is added with modest eccentricities.

The analysis with small number of eccentricities have already shown the benefit polar orbits. The solution space will be explored for SSOs where eccentricity effects are coupled with inclination.

5.2 Sun-synchronous orbits

Sun-synchronous orbits (SSO) provide a more suitable choice for reflector applications [13]. The results in the previous section is now going to be extended to SSOs, for which 1000-km altitude circular orbit (a = 7378.2 km) results are also available from Çelik & McInnes (2024) [1]. In this paper a wider semi-major axis space will be explored with two additional values, a = 7500 km and 8000 km.

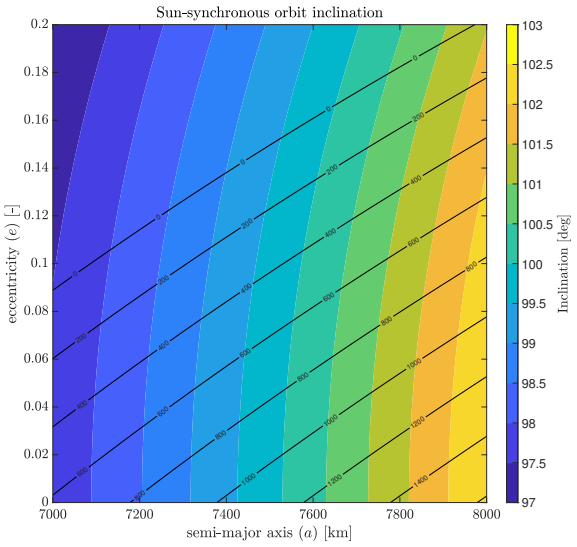

Fig. 3: Sun-synchronous orbit inclination for a given semi-major axis-eccentricity pair

In order for a comparison with circular orbits, an optimisation is performed for these two new semi-major axis values, whose results are presented in Table 5, alongside the results from Çelik & McInnes (2024) [1].

The results in Table 5 show a reduction in the quantity of energy delivered at higher altitudes, which are expected as the two larger orbits are at 1121.8 km and 1621.8 km, respectively. These are also more likely to result in overlapping passes due to the higher altitude, resulting further reduction in the post-processed results. These results will be used in comparing with elliptical results.

5.3 Grid search in eccentricity space with ω = 0

The grid search in the eccentricity space is carried out by again assuming a minimum periapsis altitude of 600 km, which results in maximum eccentricity value of 0.0696 and 0.1277 for the two larger orbits, respectively. Note that for the smallest orbit, this value is at 0.0542. The optimisation is then performed by assuming argument of periapsis value as 0 to assess the effect of the eccentricity in the final quantity of energy delivered. The results are presented in Table 6.

The solutions with fixed ω value does not demonstrate an improvement for the lowest altitude orbits, although it does demonstrate comparable performance at e=0.01. For other orbits, considerable improvement is observed across different eccentricities. The results for elliptical orbits are significantly dependent on the ω value, which determines the slant range value across the orbits. Due to the choice of solar power farm size of 10-km, the solutions for elliptical orbits are better when the orbit allows for an optimal use of the this area. For example, at a=7500 km, e=0.01 provides the best E_{tot} result because the periapsis altitude at this orbit is 1046.8 km, which result in a circular image diameter of 9.74 km, nearly filling the entire solar power farm at the zenith point. The same is also true for a = 8000 km at e = 0.075. The final, post-processed result may differ due to the overlapping passes, but they are also higher than circular orbit result for most of the cases. For the smallest orbit, this cannot be quite achieved as the circular orbit radius is already close to this optimal, therefore the best result appears at the lowest eccentricity but still lower than the circular orbit result. This results show that large orbit semi-major axis can still be selected for orbiting reflector applications and modest eccentricities can allow for higher quantity of energy dleivered to the surface, with greater flexibility. However, as shown in the polar orbit results, varying ω can improve the results further, which will be demonstrated in the next section.

5.4 Grid search in eccentricity space with free ω

The analysis in this section will focus on the effect of argument of periapsis position in the final opti-

Table 5: Optimisation results for Sun-synchronous circular orbits for comparison

a [km]	i [deg]	Ω [deg]	θ_{GMT} [deg]	E_{tot} [MWh]	$E_{tot,pp}$ [MWh]	Ref.
7378.2	99.48	92.32	27.59	537.0	363.5	[1]
7500	100.04	98.19	-2.28	507.9	303.0	This work
8000	102.63	100.42	12.26	359.2	223.8	This work

Table 6: SSO optimisation results at different eccentricities with argument of periapsis ω=0 deg.

a [km]	e [-]	i [deg]	Ω [deg]	θ_{GMT} [deg]	E_{tot} [MWh]	$E_{tot,pp}$ [MWh]
7378.2	0.01	99.47	99.6529	19.9818	457.9	355.6
7378.2	0.025	99.46	85.9543	13.1346	459.5	337.2
7378.2	0.0542	99.42	70.4922	-0.5328	399.8	294.3
7500	0.01	100.04	102.0143	-0.4654	507.4	304.3
7500	0.025	100.03	109.9981	-36.8773	455.3	318.4
7500	0.05	99.99	80.7846	4.7296	483.7	342
7500	0.0696	99.95	82.6121	5.9112	465.9	340.2
8000	0.01	102.62	105.5471	14.8901	368.8	207.8
8000	0.025	102.61	101.9895	13.1742	385.6	238.9
8000	0.05	102.56	108.0097	15.9096	405.2	234.3
8000	0.075	102.48	101.85	13.3051	428.4	239.1
8000	0.1	102.37	101.7307	13.5697	414.8	249.5
8000	0.1277	102.21	94.5603	10.2934	373.6	248.8

misation result. To analyse this, the grid of eccentricities is used in an expanded optimisation of procedure when the argument of periapsis also becomes one of the optimisation parameters. The optimisation is then carried out for each a-e pair and presented in Table 7.

When ω is freed, the results have all been improved for altitudes from an optimisation perspective, i.e. E_{tot}. The reason for these results lies again in the slant range, which is optimised with the optimal placement of the ω value for a given eccentricity. This shows that the importance of the placement of elliptical orbit in the orbital element space for this type of application. $E_{tot,pp}$ have also been improved, even if improved E_{tot} results do not necessarily guarantee this outcome. For most cases, the highest altitude orbit seem to add another pass compared to circular orbit, two passes for medium sized orbit for some eccentricities. This is approximately equivalent to 10% and 20% increase in the post-processed quantity of energy delivered for largest and medium sized orbits, respectively. Given the low number of targets (i.e., 12), this is a considerable improvement in results. Even for the smallest orbit, $E_{tot,pp}$ has now become comparable to the circular orbit results at e=0.01 and e=0.0542.

The results do not follow predictable pattern for given eccentricities. Even though the effect of eccentricity and argument of periapsis are apparent, it is not clear where the fully coupled relationship result in the most optimal orbital elements for a given altitude. Therefore the analysis will now be extended to eccentricity alongside the others for fixed semi-major axis values.

5.5 Free eccentricity and argument of periapsis

The optimisation procedure explained above is now extended to include eccentricity as a parameter to optimise. The optimisation carried out in two cases for each altitude to demonsrate a diverse cases in line with the previous results. One of them is a larger range with $e \in [0.001, e_{max}]$ based on the requirement put forward for the lowest periapsis altitude of 600 km, and two optimisation is carried for comparison with the results in the previous section with $e \in [0.1, e_{max}]$. These two cases would in principle result in six results for three semi-major axis values. But there are multiple local minima available, some result in better post-processed results than others, therefore more than six solutions are presented in Table 8.

For the smallest orbit, it is immediately apparent that the optimisation is driven to its lower bounds, at least for the first and the third result, to maximise the

Table 7: SSO optimisation results at different eccentricities with free ω.

a [km]	e [-]	i [deg]	ω [deg]	Ω [deg]	θ_{GMT} [deg]	E_{tot} [MWh]	$E_{tot,pp}$ [MWh]
7378.2	0.01	99.47	3.79	88.41	14.46	462	343.8
7378.2	0.025	99.46	324.32	87.88	12.19	471.9	318.3
7378.2	0.0542	99.42	253.23	70.31	-4.72	437.7	358.4
7500	0.01	100.04	6.75	77.81	3.076	508.9	346.0
7500	0.025	100.03	345.66	89.99	8.746	510.1	347.9
7500	0.05	99.99	324.51	109.41	1.692	497.2	324.1
7500	0.0696	99.95	280.49	81.69	0.924	509.03	364.4
8000	0.01	102.62	0.0047	107.83	16.06	368.3	240.4
8000	0.025	102.61	0.78	97.30	10.88	383.2	238.8
8000	0.05	102.56	1.33	108.36	16.16	405.1	209.2
8000	0.075	102.48	348.85	94.83	8.90	428.8	237.1
8000	0.1	102.37	344.27	101.80	12.52	440.7	239.1
8000	0.1277	102.21	331.93	100.34	11.45	438.2	244.3

Table 8: SSO optimisation results at free e and ω.

a [km]	e [-]	i [deg]	ω [deg]	Ω [deg]	θ_{GMT} [deg]	E_{tot} [MWh]	$E_{tot,pp}$ [MWh]
7372.8	0.001	99.47	0	70	0.65	472.4	356
7372.8	0.0086	99.48	343.91	82.48	10.83	458.9	353.3
7372.8	0.01	99.48	0.4382	70	-0.66	463.4	374.1
7500	0.01	100.04	3.2488	73.74	1.015	504.7	317.5
7500	0.0075	100.04	270.71	93.62	6.176	524.5	318.8
7500	0.0471	99.99	276.44	83.95	1.826	520.7	308.4
8000	0.0904	102.42	4.0896	96.81	10.90	445.2	262.2
8000	0.0973	102.38	138.99	99.96	-78.50	409.2	254.8

quantity of energy delivered. These are likely part of the same family as all other orbital elements are also similar. An interesting difference is that even though the total quantity of energy delivered E_{tot} is similar, the reflectors deliver more for the third solution in practical terms. In fact, $E_{tot,pp}$ value is higher than that of the circular orbit by 3%. This may appear small, but it provides an enhanced flexibility in mission design without loss of performance. The other solutions are also comparable to circular orbit results.

For the medium-sized orbit, the first solution is driven to its lower bounds for e, ω and Ω parameters but does not result in higher E_{tot} compared at the same eccentricity value. For the extended lower bound, there appears to be a mildly eccentric orbit with an total value 20 MWh higher at $e = 0.0075$, which is also the best solution found for this orbit case. Following this, there appears another solution with much higher eccentricity at 0.0471 with E_{tot} value of 520.4 MWh. For the post-processed results, all $E_{tot,pp}$ values are higher than that of circular orbit but not necessarily from the other eccentric orbit cases where one or two orbital elements were fixed. For the highest E_{tot} value results ($e = 0.0075$ and $e = 0.0471$), this is the smae reason as explained before: The optimisation is driven to maximise the total energy that is deliverable per day, but it does not take into account potential operational limitations over multiple solar power farms, of which only one can be serviced. There may be better $E_{tot,pp}$ solutions at other, fixed eccentricities that was shown in Table 7, for example, even though other constraints may apply those in terms of minimum periapsis altitude.

For the largest orbit, there appears two solutions that similar of nature in terms of eccentricity despite the two cases investigated. The optimal eccentricity found results in a periapsis altitude approximately 1000 km, effectively optimising solar image with respect to solar power farms and maximising the energy delivery. The solutions differ in terms of other ω and θ_{GMT}. E_{tot} values are differ and the first solution at e=0.0904 is the best solution obtained for the largest orbit. This is also true for the post-processed results.

With $E_{tot,pp}$ values of 262.2 and 254.8, the results are the best of all optimisations performed and 15-20% higher than circular orbit results.

For all different semi-major axis values, the difference in inclination is very small between different. eccentricity values. Therefore it is believed that the effect of inclination is small in the final results for the considered altitudes. If larger semi-major axis lengths and eccentricities are considered, the effect should be more apparent.

The results can also be compared by Viale et al (2022) reference architecture study [13]. Viale et al. (2022) uses a five hexagonal reflector with an equivalent diameter of 1.016 km as compared to 1 km employed in this paper and Çelik & McInnes (2024) [13, 1], at 884.6 km altitude ($a = 7262.8$ km) circular repeating groundtrack SSO [13]. The authors do not optimise orbits but "anchor" the groundtrack to Sun-Cable solar power farm (SPF-12 in this paper) and found that 283.84 MWh of solar energy can be delivered per day [13]. The circular optimal SSO at 7378.2 km presented in Table 5 already presents a significant improvement to this result, as also discussed in Çelik & McInnes (2024) [1]. In terms of circular orbits, the medium-sized orbit also presents a considerable improvement compared to Viale et al. (2022), but the same is not observed for the largest orbit. For the elliptical orbits, the results for the largest orbit improve considerably and become comparable to Viale et al. (2022), albeit still delivering less energy. Moreover, if the same reflector size is used in the largest orbit as Viale et al. (2022) (i.e., 1.016 km diameter), the area would have been increased by approximately 3.22%, yielding an increase in the energy delivery by the same quantity, i.e., from 262.2 MWh to 270.1 MWh, according to the discussion in Sec. 2, resulting a comparable energy delivery. These results show that the limitations of higher altitude circular orbits in terms of orbiting reflector applications can be mitigated and in fact improved by employing elliptical orbits with or without increasing the reflector size. A further increase in the quantity of energy delivered can be obtained by expanding this single orbit results to constellations, which will be discussed next.

6. Discussion: Orbiting Solar Reflector Constellations

The results presented in earlier sections can now be expanded to a full constellation. A small number of 10 reflector satellites are considered for this discussion. As discussed in Sec. 3, the reflectors can be placed and synchronised with the Earth's rotation and oblateness effect in such a way that they would all follow over a ground target. In that case, only Ω and mean anomaly of the orbits would need to be altered while the rest of the orbital elements would be same. In this case, a phase angle $\phi = 15$ deg is selected to place the satellites. An illustration of the constellation is shown in Fig. 4 from the results in Table 8.

From the figures, it is possible to observe that reflectors are approximately 15 deg apart from each other. Particularly for the largest orbit, the ellipticity is apparent. All reflectors are away from the Earth's shadow, which validates the aim of constellations to be away from eclipses.

The favourable placement of the reflector's in subsequent orbits mean that the quantity of energy delivered can be scaled linearly with given number of reflectors, i.e., $E = NE_{tot}$, where N is the total number of reflector satellites. The post-processed total daily quantity of energy delivered will be used for this analysis. For N=10, the total quantity of energy delivered per day is equal to 3741 MWh for a=7378.2 km, 3188 MWh for a=7500 km and 2622 MWh a=8000 km orbits, respectively. Approximately 10% of the solar energy delivered can be converted to electricity with the current terrestrial solar energy technology. Compared to respective circular orbit cases with the same number of satellites, this represents 3%, 4.5% and 17% increase for each orbit considered, respectively. Note that the for the former two values the eccentricities are very modest (0.01 and 0.0075, respectively) and the percentage increase is much higher for the original, unprocessed optimisation outcome. The results demonstrate that between circular and very modest eccentricities, a performance increase is possible, mitigating some of the altitude constraints for orbiting reflector applications.

It was discussed previously in Çelik & McInnes (2024) that a constellation of ten orbiting reflectors at 1000-km altitude circular SSO can enable electricity generation equivalent to a terrestrial solar power farm, albeit distributed globally [1]. The same discussion can be extended to the constellations discussed here. Particularly for the smallest orbit, elliptical orbits represent a further improvement. For the mid-sized orbit, the quantitative result is similar to the smallest orbit in the elliptic case, despite the higher semi-major axis length. The largest orbit is smaller compared to the other two but still high compared to equivalent circular orbit. An important point to note that these results are based on a single reflector size for all orbit sizes. Larger orbit radii typically require

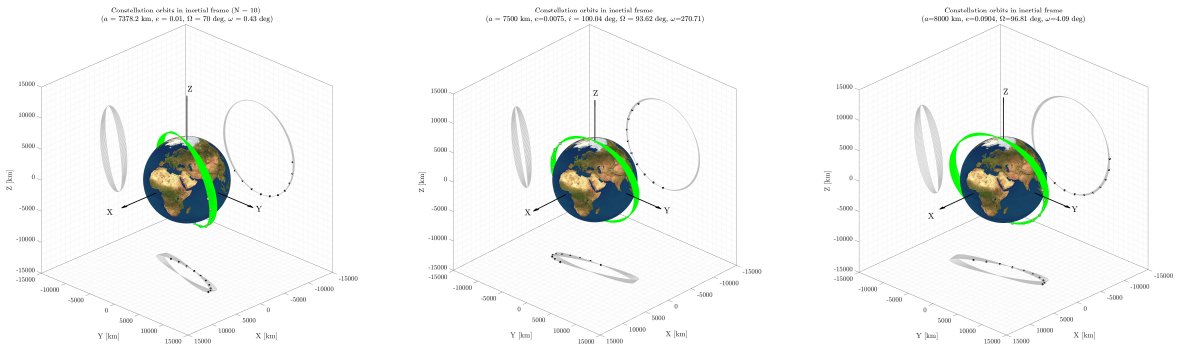

(a) a=7378.2 km (b) a=7500 km (c) a=8000 km

Fig. 4: An illustration of the constellations at three different semi-major axis cases from Table 8 with ϕ=15 deg.

less control torques, therefore larger reflectors can be accommodated for a controller in circular orbits [31]. Elliptical orbits complicate this interpretation due to varying instantaneous distance from the Earth, but nevertheless, the quantity of energy delivered can be increased further by larger reflectors.

Large reflector in low-Earth orbit (LEO) space face increased collision with space debris and atmospheric drag even at relatively higher altitudes compared to conventional smaller sized satellites. The LEO environment is the most congested between 700-1000 km SSO zone, and poses a significant danger to orbiting reflectors missions considered in this region [13, 1, 21]. Smaller size, higher number of reflectors may be considered for lowered individual collision risk and altitude loss due to drag, but the mission lifetime can be extended further by avoiding these altitudes all together, at least for a portion of the orbit. Elliptical orbits enable such a strategy without loss of performance and often improvements. Implementation of such a strategy could significantly enhance the flexibility in mission design for orbiting reflector, which can also be combined with other strategies such as smaller reflectors. Elliptical orbits may also be considered for temporary orbits to avoid a collision risk, staging orbits for constellation reconfiguration, more heterogenous constellations mixing different types of orbits to optimise energy delivery to smaller solar power farms, which are more common, or to deliver energy from multiple orbit shells, adjusting solar power density in certain hours of the day and deliver energy for a longer pass duration for global clean energy generation.

7. Conclusions

Terrestrial solar energy generation can be enhanced by employing constellations of orbiting solar reflector that locally illuminate solar power farms. Circular orbit constellations have previously shown as promising candidates for scalable, predictable and continuous solar energy delivery but the altitude dependency of the quantity of energy delivered limits the choice of orbits considerably. Instead elliptical orbits can provide greater flexibility in mission design little to no performance loss. This paper therefore investigates the effectiveness of elliptical orbits in the design of orbiting reflector constellations.

The constellation design is simplified by using an analytical formulation that distributes the satellites in the right ascension of the ascending node space such that each satellite follows the same groundtrack. This means that a single orbit optimisation is sufficient to describe the constellation. This optimisation is performed by a genetic algorithm with an objective to maximise the total quantity of energy delivered per day to 12 existing solar power farm. Initial analysis performed by polar orbits to remove eccentricity-inclination coupling in the Sun-synchronous orbits (SSO) and it was found that modest eccentricity can increase the value of the objective function compared to circular orbits. Part of this result is due to the opportunity to tune the eccentricity in such a way that solar energy delivery is maximised to notional disk shaped solar power farms. The analysis with SSOs is conducted in multiple steps by a grid search in eccentricity with an initially fixed and later free argument of periapsis value, which is later extended to free eccentricity for three different semi-major axis

values. In all cases considered, a significant improvement has been observed in the final quantity of total energy delivered with respect to circular orbit results. However, this means that some overlapping passes exist between closely located solar power farms, which may mean that, in reality, there would be less power delivered that the optimisation results. Nevertheless, the consideration of elliptical orbits would provide enhanced flexibility in mission design, particularly in terms of avoiding enhanced atmospheric drag and space debris fields in low-Earth orbit space, often with improvements in performance up to 20%.

This paper has only considered a limited set of orbits for the effectiveness of the elliptical orbits without operational considerations within the optimisation. Inclusion of greater set of orbits and the selection of serviceable solar power farms during could yield even more improved results. Nevertheless, the methodology can be applied to any constellation design applications beyond space-based solar power and the results demonstrate the benefits of elliptical orbits for enhanced performance for constellations in general and for the delivery of truly global clean energy from space.

Acknowledgments

References

[1] O. Çelik, C. R. McInnes, A constellation design for orbiting solar reflectors to enhance terrestrial solar energy, Acta Astronautica 217 (2024) 145–161. doi:10.1016/j.actaastro.2024.01.031.

[2] O. Çelik, A. Viale, T. Oderinwale, L. Sulbhewar, C. R. McInnes, Enhancing terrestrial solar power using orbiting solar reflectors, Acta Astronautica 195 (2022) 276–286. doi:10.1016/j.actaastro.2022.03.015.

[3] M. Berthet, J. Schalkwyk, O. Çelik, D. Sengupta, K. Fujino, A. M. Hein, L. Tenorio, J. Cardoso dos Santos, S. P. Worden, P. D. Mauskopf, Y. Miyazaki, S. Tsuji, P. Fil, K. Suzuki, Space sails for achieving major space exploration goals: historical review and future outlook, Progress in Aerospace Sciences 150 (101047) (2024). doi:10.1016/j.paerosci.2024.101047.

[4] M. Berthet, D. Sengupta, O. Çelik, A. Hein, K. Fujino, J. Schalkwyk, L. Tenorio, J. C. dos Santos, Database on space sails, mendeley Data (2024). doi:110.17632/pr6pk3xmsp.3.

[5] H. Oberth, Methods of space travel, Munich, Oldenburg (1929) 494.

[6] P. E. Glaser, Power from the sun: Its future, Science 162 (3856) (1968) 857–861. doi:10.1126/science.162.3856.857.

[7] K. W. Billman, W. P. Gilbreath, S. W. Bowen, Introductory assessment of orbiting reflections for terrestrial power generation, Tech. Rep. NASA-TM-73230, NASA (1977).

[8] J. E. Canady, J. L. Allen, Illumination from space with orbiting solar-reflector spacecraft, Tech. Rep. NASA-TP-2065, NASA (1982).

[9] K. A. Ehricke, Space light: space industrial enhancement of the solar option, Acta Astronautica 6 (12) (1979) 1515–1633. doi:10.1016/0094-5765(79)90003-1.

[10] V. A. Koshelev, V. M. Melnikov, Large Space Structures Formed by Centrifugal Forces, Earth Space Institute Book Series, CRC Press, Boca Raton, FL, 1998. doi:10.1201/9781000124699.

[11] L. M. Fraas, M. J. O'Neill, Sunbeams from Space Mirrors for Terrestrial PV, Springer International Publishing, Cham, 2023, pp. 163–176. doi:10.1007/978-3-031-30812-3_12.

[12] F. Bonetti, C. McInnes, Space-enhanced terrestrial solar power for equatorial regions, Journal of Spacecraft and Rockets 56 (1) (2019) 33–43. doi:10.2514/1.A34032.

[13] A. Viale, O. Çelik, T. Oderinwale, L. Sulbhewar, C. R. McInnes, A reference architecture for orbiting solar reflectors to enhance terrestrial solar power plant output, Advances in Space Research 72 (4) (2023) 1304–1348. doi:10.1016/j.asr.2023.05.037.

[14] A. Viale, O. Çelik, T. Oderinwale, L. Sulbhewar, G. Bailet, C. R. McInnes, Towards the commercial development of orbiting reflectors: a technology demonstration roadmap, in: 73rd International Astronautical Congress (IAC 2022), IAF, Paris, France, 2022, paper no. IAC–22–C3.2.x70070.

[15] R. Bewick, J. P. Sanchez, C. R. McInnes, Use of orbiting reflectors to decrease the technological challenges of surviving the lunar night, in: 62nd International Astronautical Congress (IAC 2011), Vol. 2, IAF, Cape Town, South Africa, 2011, pp. 1597–1609, paper no. IAC-11-A5.1.11.

[16] O. Çelik, C. R. McInnes, Enhancing planetary exploration using orbiting solar reflectors, in: 45th COSPAR Scientific Assembly, COSPAR, Busan, South Korea, 2024.

[17] O. Çelik, C. R. McInnes, An investigation into a combined service of space-based solar energy and climate engineering via orbiting solar reflectors, in: 75rd International Astronautical Congress (IAC 2022), IAF, Milan, Italy, 2024, paper no. IAC-24-D1,1,12,x83911.

[18] J. G. Walker, Satellite Constellations, Journal of the British Interplanetary Society 37 (1984) 559.

[19] O. Çelik, C. R. McInnes, An analytical model for solar energy reflected from space with selected applications, Advances in Space Research 69 (1) (2022) 647–663. doi:10.1016/j.asr.2021.10.033.

[20] O. Çelik, C. R. McInnes, A generic three-dimensional model for solar energy reflected from mirrors in circular orbits, Advances in Space Research (2023). doi:10.1016/j.asr.2023.09.046.

[21] R. Gordon, C. R. McInnes, End-of-life considerations for orbital solar reflectors, in: Proceedings of the 35th AAS/AIAA Space Flight Mechanics Meeting, Kaua'i, Hawaii, 2025.

[22] J. E. Draim, et al., Elliptic orbit constellations: a new paradigm for higher efficiency in space systems, Acta Astronautica 51 (9-10) (2002) 475–489. doi:10.1016/S0094-5765(02)00036-X.

[23] V. N. Doniants, Y. P. Ulybyshev, Elliptic orbit constellations for regional communication and molniya-zond satellite constellation, in: 53rd International Astronautical Congress, IAF, Houston, TX, 2002.
URL https://ui.adsabs.harvard.edu/abs/2002iaf..confE.604D/abstract

[24] L. Wood, Y. Lou, O. Olusola, Revisiting elliptical satellite orbits to enhance the o3b constellation, arXiv preprint (2014). arXiv:1407.2521.
URL https://arxiv.org/abs/1407.2521

[25] D. Kim, T. Chung, Design of an elliptical orbit constellation for high-resolution optical observations over a specific area, Journal of Astronomy and Space Sciences 40 (3) (2023) 191–203. doi:10.1007/s42405-023-00690-5.
URL https://link.springer.com/article/10.1007/s42405-023-00690-5

[26] D. Mortari, M. P. Wilkins, C. Bruccoleri, The flower constellations, The Journal of the Astronautical Sciences 52 (2004) 107–127. doi:10.1007/BF03546424.

[27] H. C. Hottel, A simple model for estimating the transmittance of direct solar radiation through clear atmospheres, Solar energy 18 (2) (1976) 129–134. doi:10.1016/0038-092X(76)90045-1.

[28] H. Yi, W. Lei, F. Wenju, Z. Haitao, L. Tao, X. Beizhen, C. Ruizhi, Leo navigation augmentation constellation design with the multi-objective optimization approaches, Chinese Journal of Aeronautics 34 (4) (2021) 265–278. doi:10.1016/j.cja.2020.09.005.

[29] V. A. Chobotov, Orbital mechanics, AIAA, 2002. doi:https://doi.org/10.2514/4.862250.

[30] D. E. Goldberg, Genetic Algorithms in Search, Optimization and Machine Learning, Addison-Wesley Longman Publishing Co., Inc., 1989.

[31] A. Viale, C. R. McInnes, Attitude control actuator scaling laws for orbiting solar reflectors, Advances in Space Research 71 (1) (2023) 604–623. doi:10.1016/j.asr.2022.10.015.